Nuclear Instruments and Methods in Physics Research B 101 (1995) 499–510

ELSEVIER

NIM B
Beam Interactions with Materials & Atoms

A simple model of photon transport

Dermott E. Cullen *

Lawrence Livermore National Laboratory, L-294, P.O. Box 808, Livermore, CA 94550, USA

Received 30 September 1994; revised form received 3 March 1995

Abstract

In this paper I describe a simple model of photon transport. This simple model includes: tabulated cross sections and average expected energy losses for all elements between hydrogen ($Z = 1$) and fermium ($Z = 100$) over the energy range 10 eV to 1 GeV, simple models to analytically describe coherent and incoherent scattering, and a simple model to describe fluorescence. This is all of the data that is required to perform photon transport calculations.

1. A simple model

The following sections will discuss the details of each component of the simple model. These components include: (1) integral parameters: cross sections and average expected energy deposits, (2) photon scattering, coherent form factors and incoherent scattering functions, (3) fluorescence, and (4) pair and triplet production.

1.1. Treatment of integral parameters

In this section, I discuss the treatment of integral parameters, which includes: total photoelectric, coherent and incoherent scattering, pair and triplet production cross sections, photoelectric subshell cross sections, and expected energy deposition for photoelectric, incoherent scattering, pair and triplet production.

The data used is based on the Livermore Evaluated Photon Data Library (EPDL), which includes data for all elements between hydrogen ($Z = 1$) and fermium ($Z = 100$), over the energy range 10 eV to 100 GeV [1]. This data has been adopted as the ENDF/B-VI Photon Interaction Library [2], but at the request of the Cross Section Evaluation Working Group (CSEWG), the ENDF/B-VI data has been restricted to the energy range 10 eV to 100 MeV.

In addition to the basic integral cross sections describing coherent, incoherent, photoelectric, pair and triplet production, EPDL also includes photoelectric cross sections for each atomic subshell and expected energy deposits for each process. EPDL also includes form factors and scattering functions to describe coherent and incoherent scattering, respectively. The ENDF/B-VI library includes the photoelectric subshell cross sections, form factors and scattering functions, but not expected energy deposits (there are no ENDF/B formats for these quantities).

In evaluating the EPDL data, each physical process for each element was considered separately. The result is data represented on a different energy grid for each process and each element and generally requiring log–log interpolation between the tabulated results. Using this data in this form in applications would be extremely cumbersome, very expensive and simply not practical.

For use in applications the data has been reduced to simple tabulated form. For each element, all cross sections and average expected energy deposits are all in a simple tabulated form where all parameters are tabulated at the same energies and the tabulated energy points have been selected to allow linear interpolation to any energy between any two tabulated points. At the request of users, the energy range has been extended from the ENDF/B-VI upper limit of 100 MeV, up to 1 GeV.

Once the data for each element has been reduced to the simple tabulated form, described above, where all parameters are represented on exactly the same energy grid, and can be accurately represented using linear interpolation between tabulated points, a very efficient and almost trivial binary search can be used to define the tabulated energy interval within which the current energy lies. Once this is done, ALL of the parameters for an element can be defined as a simple weighted sum of the contributions from the two tabulated values at the ends of the interval. For example, assume that the current energy, E, lies between the tabulated energies, E_{j-1} and E_j. If we define the weights,

$$\text{Weight}_j = \frac{E - E_{j-1}}{E_j - E_{j-1}}, \qquad \text{Weight}_{j-1} = 1 - \text{Weight}_j, \tag{1}$$

* Tel. +1 510 423 7359, fax +1 510 422 9523, e-mail cullenl@llnl.gov.

0168-583X/95/$09.50 © 1995 Elsevier Science B.V. All rights reserved
SSDI 0168-583X(95)00480-7

then ANY and ALL parameters can be defined at energy, E, as,

$$F(E) = \text{Weight}_j F_j + \text{Weight}_{j-1} F_{j-1}, \quad (2)$$

where F is any parameter of interest, e.g., photoelectric or pair production cross section, incoherent or photoelectric energy deposit, K or L1 photoelectric subshell cross section, etc. and F_{j-1}, and F_j are the tabulated values of F at E_{j-1} and E_j, respectively.

The systematic variation of the photoelectric edges as a function of atomic number (Z) does not allow the data for all of the elements to be accurately represented on a common energy grid for all elements.

To represent all of the data over the entire energy range from 10 eV up to 1 GeV and allow accurate linear interpolation between tabulated points requires no more than 255 points for any given element. In creating the files, no attempt was made to keep the number of points under this limit; it just happened naturally. But the result is obviously ideal for facilitating a quick and efficient binary search.

Formerly, people have attempted to fit the photon interaction cross sections to analytical expressions that could be used in applications. This approach worked quite well to represent the basic cross sections and has been very successfully used in the past.

If we wish to perform more detailed photon transport calculations where we require more detailed information, such as photoelectric subshell cross sections, over more extended energy ranges, the approach of using analytical expressions becomes impractical.

In the case of the approach used here, a combination of 19 different cross sections and energy depositions can ALL be defined at any given energy as this simple weighted average of two tabulated terms. If one attempted to fit all of this data to analytical expressions and then had to evaluate each of the analytical expressions at each energy during a transport calculation, it seems clear which approach would be both faster and more accurate, i.e., the old approach of using analytical expressions simply is not practical to use for more detailed calculations.

1.2. Photon scattering

In the following sections, discussing photon scattering, we will only be interested in developing methods to efficiently sample the normalized scattering distributions. We assume that the cross section for each process has already been defined and what we are interested in is: given that a coherent or incoherent scattering event has occurred (based on the cross sections), what is the angular, and in the case of incoherent also the energy, distribution of the scattered photons.

Below, we will see that based on the equations describing coherent and incoherent scattering, the most "natural" angular variable to use is neither angle nor cos, but rather $1 - \cos$; and more generally $E^2(1 - \cos)$, where cos is the cosine of the photon scattering angle.

1.3. Coherent scattering

The angular distribution of coherently scattered photons is a product of Rayleigh scattering and a correction factor,
sig(cos) = R(cos) $f(E,\cos)$,
R(cos) = Rayleigh scattering,
$f(E,\cos)$ = correction factor,
E = incident photon energy,
cos = photon scattering cosine,
FF(E,cos) = the form factor,
AS(E) = the anomalous scattering factor:

$$R(\cos) = [\cos^2 + 1],$$

$$f(E,\cos) = [\text{FF}(E,\cos) + \text{AS}(E)]^2. \quad (3)$$

The anomalous scattering factor plays an important role by creating minima in the coherent scattering cross section just below photoelectric edges and in causing the coherent scattering cross section to approach zero as E^2 as energy approaches zero [3].

It plays a less important role in that it effects the angular distribution of coherently scattered photons near photoelectric edges.

The important effect of the anomalous scattering factor on the coherent cross section has been included in the EPDL cross sections. The less important effect of the anomalous scattering factor on the angular distributions near photoelectric edges will be ignored here; so that we assume,

$$f(E,\cos) = \text{FF}(E,\cos)^2 = \text{form factor squared.} \quad (4)$$

Generally for use in applications, the form factor is represented in tabulated form that is then fit by some procedure (e.g., cubic spline) and sampled.

Here we will use an analytical expression that is simple, accurate and more efficient to sample.

For a hydrogen atom the form factor is [4,5],

$$\text{FF}(E,\cos) = \frac{Z}{[1 + Bx]^2}, \quad x = E^2(1 - \cos), \quad Z = 1,$$

for hydrogen. (5)

For more complicated atoms, the form factor can be represented by a sum of terms, with each term corresponding to the contribution of each atom subshell, j,

$$\text{FF}(E,\cos) = \sum_j \frac{A_j}{[1 + B_j x]^{Nj}}, \quad (6)$$

so that the form factor squared, that we need for use in applications, can be represented in the form,

$$\text{FF}(E,\cos)^2 = \sum_j \frac{A_j}{[1 + B_j x]^{Nj}} \sum_k \frac{A_k}{[1 + B_k x]^{Nk}}. \quad (7)$$

This form is judged to be too complicated and expensive to use in Monte Carlo calculations. So we will use the pragmatic approach of representing the form factor in the form,

$$\mathrm{FF}(E,\cos)^2 = \sum_j \frac{A_j}{\left[1+B_j x\right]^N}, \tag{8}$$

and use A_j, B_j and N as free parameters to fit tabulated form factors. N is easily defined by examining the high energy shape of the form factor, where,

$B_j x \gg 1$,

in which case the shape is given by,

$$\sum_j \frac{A_j}{\left[1+B_j x\right]^N} = \frac{C}{x^N}, \tag{9}$$

where

$$C = \sum_j \frac{A_j}{B_j^N},$$

so that N is merely the high energy log slope of the form factor. A_j and B_j are then defined to obtain the best fit to the form factor.

In the normally used definition of the form factor, it varies from Z at low energy to 0 at high energy. Since here we are fitting the square of the form factor, the one constraint that we have is,

$$Z^2 = \sum_j A_j. \tag{10}$$

It has been found that the tabulated EPDL form factors can be very accurately fit using no more than a sum of three terms. For hydrogen and helium where we only have one atomic shell (K), only one term is required. For $Z = 3$ to 10, we have K and L shells, and only two terms are required. For higher Z elements more terms are required as the effect of each subshell can be seen. However, since generally coherent scattering is described as an interaction between a photon and the inner most, most tightly bound electrons of an atom we do not see a sum corresponding to contributions from each subshell; the sum seems to saturate and involve contributions from only up to three discernible terms. The power N varies smoothly from 4 for hydrogen ($Z = 1$) to about 2.43 for fermium ($Z = 100$).

Figs. 1 and 2 illustrate comparisons between the original EPDL form factors and the fits that can be used in applications. These figures illustrate results for elements

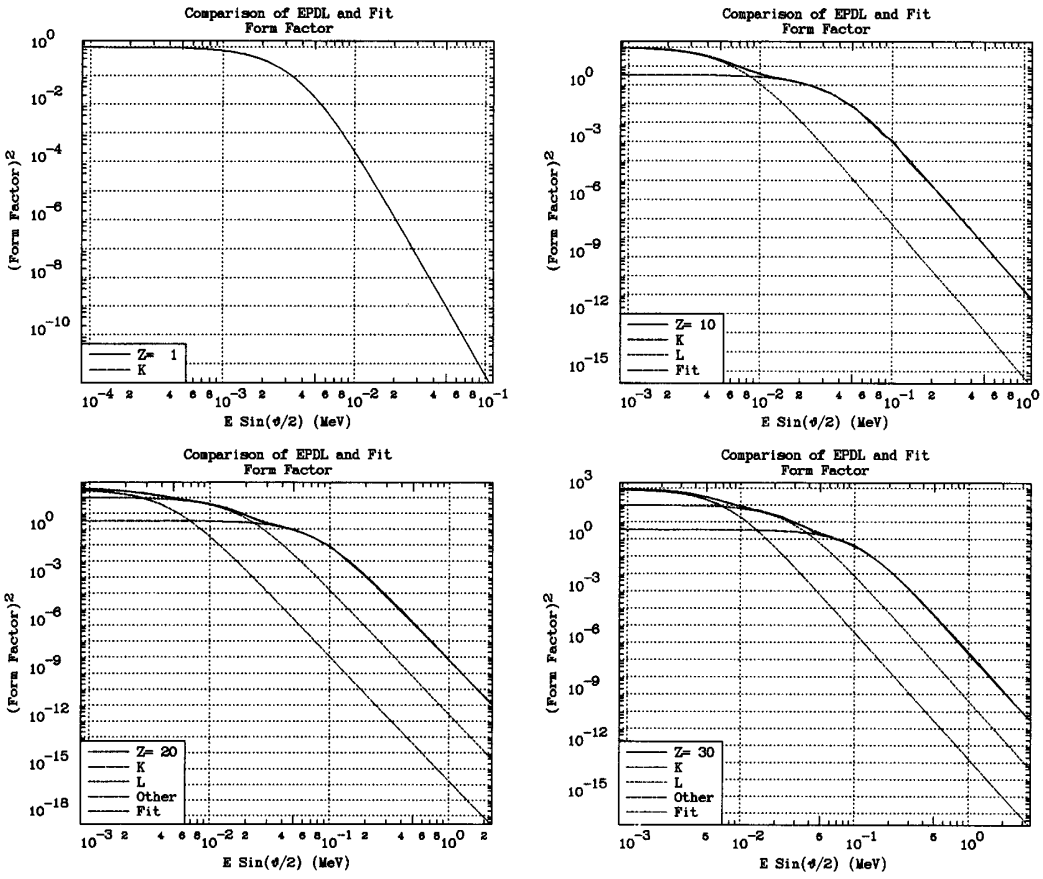

Fig. 1. Comparison of EPDL and fit form factor.

across the periodic table, $Z = 1$, 10, 20, 30, 40, 60, 80 and 100. The results indicate that these simple fits can be used to approximate the square of the form factor over ten to twelve decades of variation, i.e., well beyond the range that we can normally statistically sample.

As can be seen from these figures, at low energy the form factor is virtually isotropic and sampling only involves sampling the Rayleigh cross section. However, at higher energies the form factors are very strongly forward peaked and dominate the definition of the angular distribution of coherently scattered photons.

This suggests using a rejection technique to first analytically sample the form factor and then accept or reject based on the Rayleigh cross section.

The integral of each term of our fit is,

$$P' = \int_0^{y'} \frac{A_j \, dy}{\left[1 + B_j E^2 y'\right]^N}, \tag{11}$$

$$= \frac{A_j \left[\left(1 + B_j E^2 y\right)^{N-1} - 1\right]}{(N-1) B_j E^2 \left[1 + B_j E^2 y\right]^{N-1}}. \tag{12}$$

The normalization is defined by setting $y = 1 - \cos = 2$.

The normalization can be calculated in advance for each of the terms of the fit as a function of incident energy at the same energies at which the cross sections are tabulated. Then when a coherent scatter occurs, the tabulated normalization can be used to quickly randomly select one of the three terms based on its normalization, i.e., its contribution to the sum of terms.

From this point on, we need only be concerned with randomly sampling the one term of the series that we have selected. The normalized form for one term is,

$$P = \frac{1 - \dfrac{1}{\left[1 + B_j E^2 y\right]^{N-1}}}{1 - \dfrac{1}{\left[1 + B_j E^2 2\right]^{N-1}}}, \tag{13}$$

P = a random number, 0 to 1.

The scattering angle is then defined by analytically inverting and solving for y ($y = 1 - \cos$).

Select a random number, P, in the range 0 to 1, and define,

$Q = B_j E^2$,

$D = 1 + 2Q$,

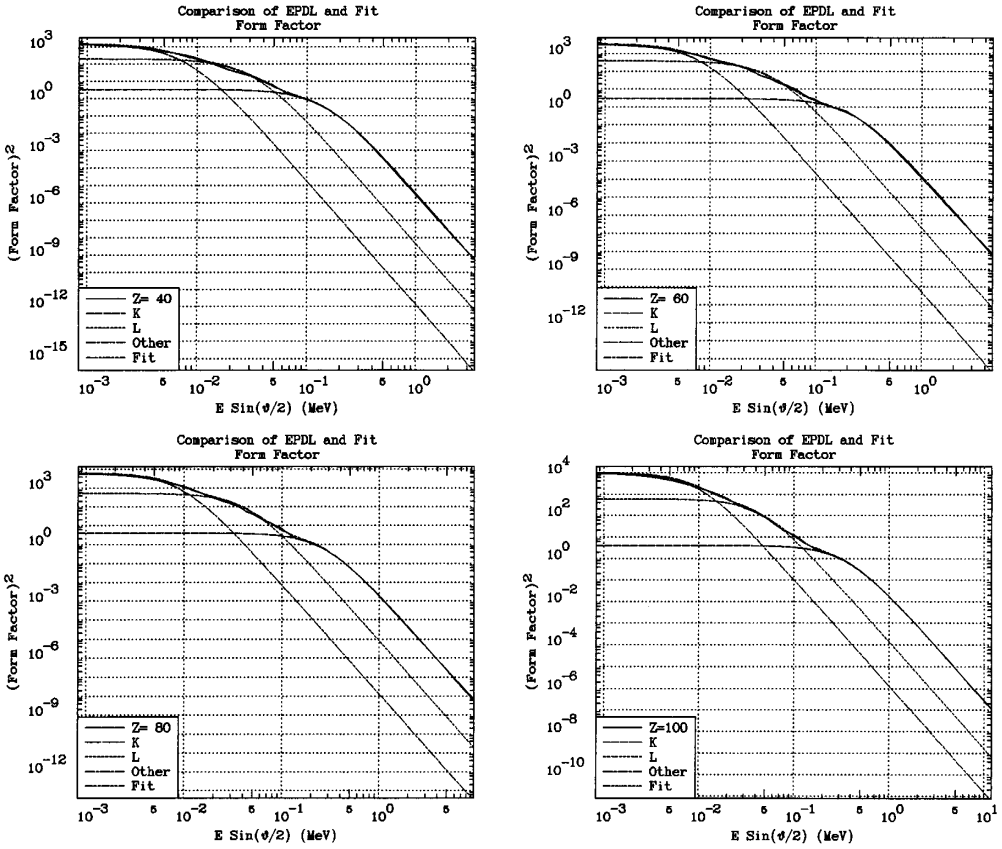

Fig. 2. Comparison of EPDL and fit form factor.

$$F = \left[P + (1-P)D^{N-1}\right]^{[1/(N-1)]}, \quad (14)$$

$$y = \frac{[D-F]}{[QF]}.$$

The two limits of $P = 0$ and $P = 1$ can be easily seen to correspond to, cos = +1 and −1, respectively.

Lastly accept or reject based on the Rayleigh cross section; an energy independent efficiency of 66% (i.e., 2/3).

1.4. Incoherent scattering

The angular distribution of incoherently scattered photons is a product of the scattering function and the Klein–Nishina formula,

$$\text{sig(cos)} = \text{SF}(E,\text{cos})\text{KN}(E,\text{cos}), \quad (15)$$

SF(E,cos) = the scattering function,
KN(E,cos) = Klein–Nishina formula

$$= C\left(\frac{A'}{A}\right)^2\left[\left(\frac{A}{A'}\right) + \left(\frac{A'}{A}\right) - 1 + \cos^2\right], \quad (16)$$

A = photon incident energy in electron rest mass units.

The energy of the scattered photon is,

$$A' = \frac{A}{[1+Ax]}, \quad x = 1 - \cos. \quad (17)$$

Substituting for A' and canceling terms we find,

$$\text{KN}(E,\text{cos}) = \frac{[1+\cos^2][1+Ax] + [Ax]^2}{[1+Ax]^3},$$

$$x = 1 - \cos. \quad (18)$$

Note, at low energy as A approaches zero, the Klein–Nishina equation approaches Rayleigh scattering,

$$\text{KN}(E,\text{cos}) \rightarrow [1+\cos^2], \quad (19)$$

and the energy of the scattered photon approaches that of the incident photon, i.e., the energy loss approaches zero and incoherent scattering approaches coherent scattering.

As in the case of coherent scattering, we will use an analytical expression to represent the scattering function. For hydrogen we have the relationship,

$$\text{SF}(E,\text{cos}) + \text{FF}(E,\text{cos})^2 = 1. \quad (20)$$

Although this is strictly not valid for other elements it

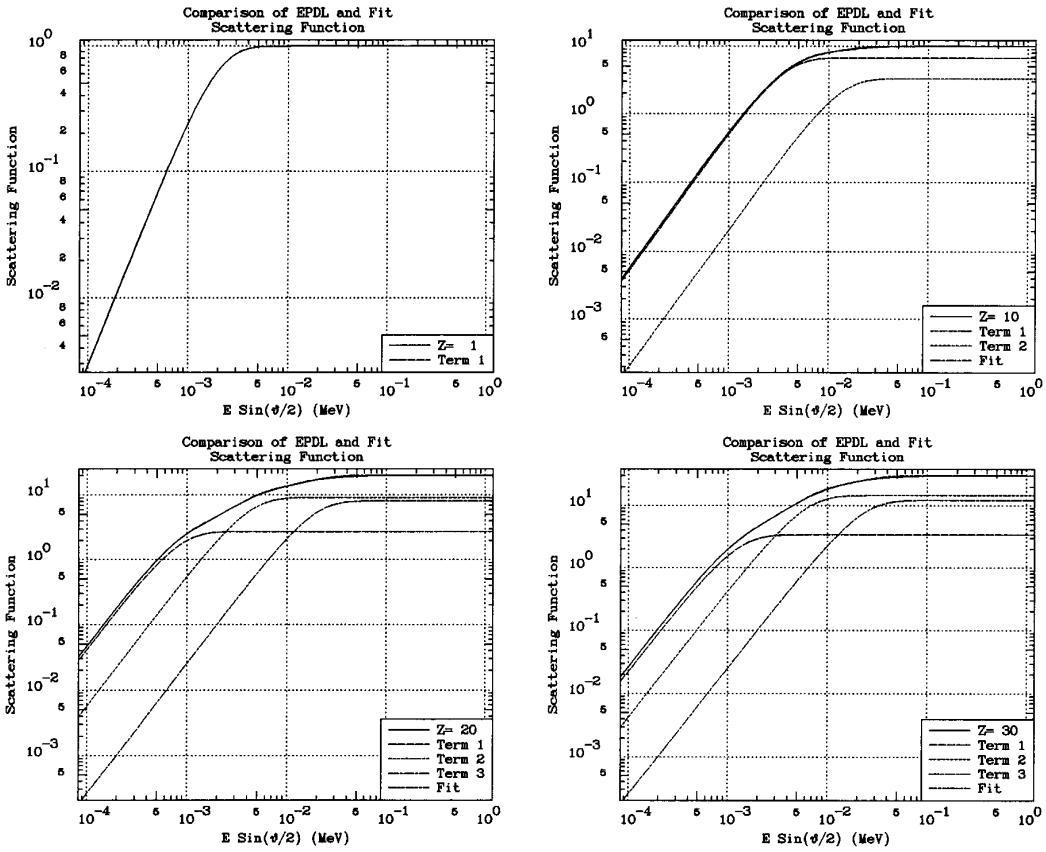

Fig. 3. Comparison of EPDL and fit scattering function.

is often used as an approximation. However, this suggests using,

$$\mathrm{SF}(E,\cos) = Z - \mathrm{FF}', \tag{21}$$

where FF′ has the same functional form as our fit for the form factor squared,

$$\mathrm{FF}' = \sum_j \frac{A_j}{\left[1+B_j x\right]^N}. \tag{22}$$

For each element we will use the same value of N as previously defined for the form factor squared, and A_j and B_j will be treated as fitting parameters. Note A_j and B_j here need not be the same as those defined for coherent scattering, e.g., for coherent scattering the sum of the A_j is Z^2, whereas here it is Z. However, when rescaled for this difference, they are very similar as predicted by Eqs. (20) and (21); for hydrogen they are virtually identical.

At low energy the scattering function approaches zero as E^2 in the forward direction and at high energies it approaches a constant, Z, in the backward direction; indeed in almost all directions, except the extreme forward direction.

For the normally used definition of the scattering function, it varies from 0 at low energy to Z at high energy. Therefore the one constraint that we have is,

$$Z = \sum_j A_j, \tag{23}$$

and we can write

$$\mathrm{SF}(E,\cos) = Z - \sum_j \frac{A_j}{\left[1+B_j x\right]^N} = \sum_j A_j \left\{1 - \frac{1}{\left[1+B_j x\right]^N}\right\}. \tag{24}$$

The results are similar to those obtained for coherent scattering, in the sense that it has been found that in no case are more then three terms required to obtain excellent agreement between the EPDL scattering functions and the fit. One term is adequate for $Z = 1$ or 2, where we only have one shell (K). Two terms are required for $Z = 3$ to 10, where we have two shells (K, L). Higher Z elements require an additional term. Incoherent scattering is usually described as an interaction between a photon and the outer most, most loosely bound electrons. So what we seem to

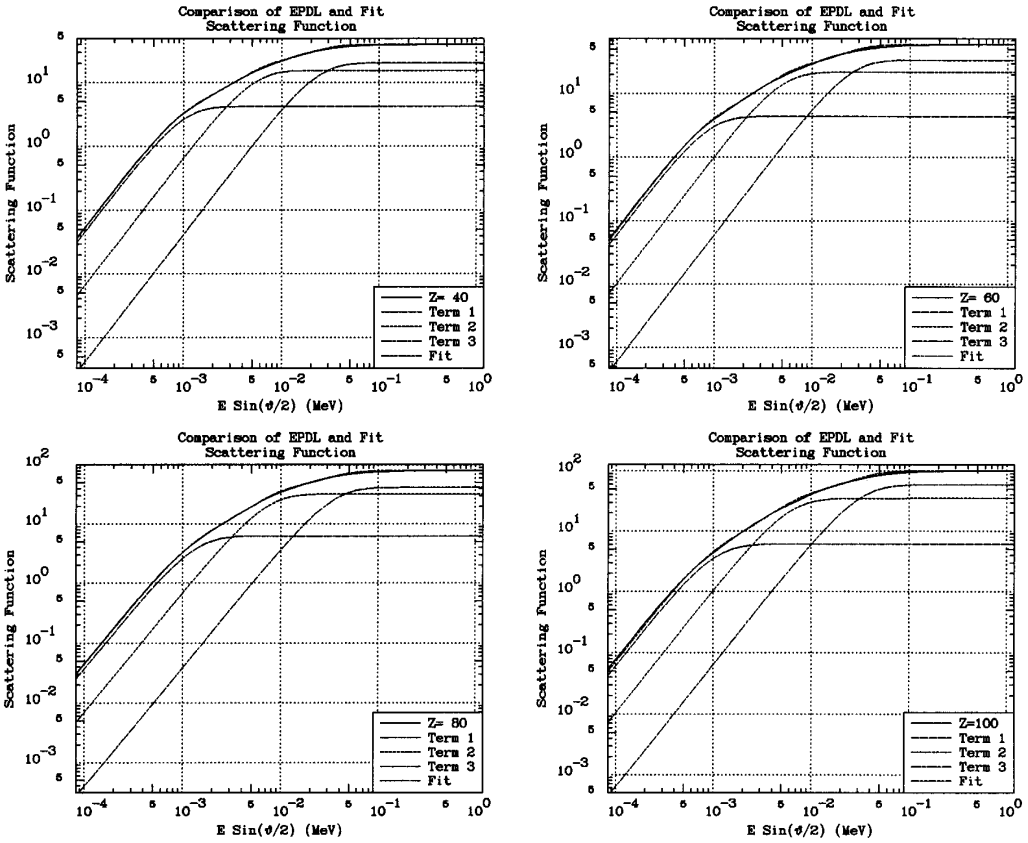

Fig. 4. Comparison of EPDL and fit scattering function.

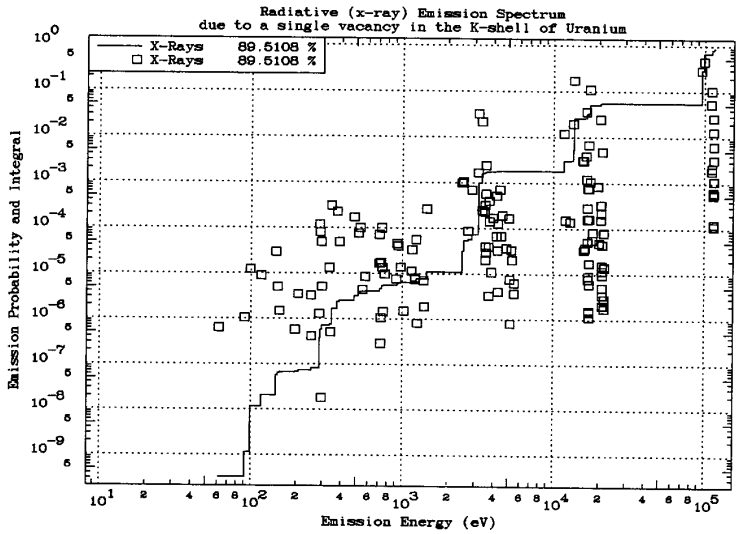

Fig. 5. Radiative (X-ray) emission spectrum.

see is that the sum rather than including contributions from each subshell, saturates and only requires up to three terms to represent the contribution of the outer most subshells.

Figs. 3 and 4 illustrate comparisons between the original EPDL scattering functions and the fits that can be used in applications.

At low energies the scattering function plays an important role in suppressing forward scattering, compared to the Klein–Nishina formula. In the case of extreme low energies it essentially multiplies the Klein–Nishina formula by E^2. At higher energies the scattering function plays very little role, except at very forward angles where it will always suppress the forward scattering. At very high energies it plays essentially no role and is often simply ignored in applications.

This suggests using a rejection technique to first sample the Klein–Nishina formula and then accept or reject based on our fit. In this case we need not invert our fit (as was

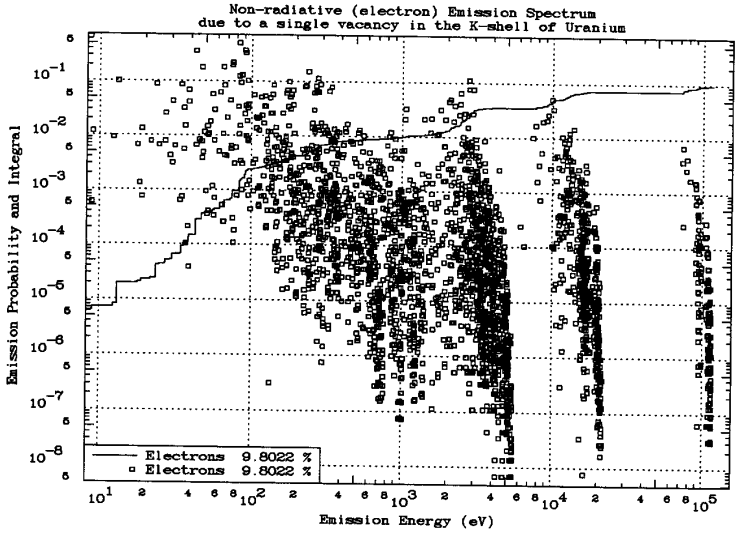

Fig. 6. Nonradiative (electron) emission spectrum.

done in the case of coherent scattering), we merely first sample the Klein–Nishina formula to define x and then define the sum,

$$\mathrm{SF}(E,\cos) = \sum_j A_j \left\{ 1 - \frac{1}{\left[1 + B_j x\right]^N} \right\}, \tag{25}$$

and accept if the sum is greater than or equal to Z times a random number. The efficiency will vary from $1/3$ at low energy to essentially 1 (100% acceptance) at high energies.

1.5. Fluorescence

The Livermore Evaluation Atomic Data Library (EADL) (see Ref. [1]) contains data to describe the relaxation of atoms back to neutrality after they are ionized, regardless of what physical process ionized the atom, e.g., photoelectric, electron ionization, internal conversion, etc.

The data in EADL includes the radiative and non-radiative transition probabilities for each subshell of each element, for $Z = 1$ through 100. Given that an atom has been ionized by some process that has caused an electron to be ejected from an atom, leaving a vacancy or "hole" in a given subshell, the EADL data can be used to calculate the complete radiative (fluorescence) and non-radiative (Auger and Coster–Kronig) spectrum of X-rays and electrons emitted as the atom relaxes back to neutrality [6].

For a K shell photoelectric event in uranium if fluorescence is not considered all of the energy of the photon is assumed to be deposited locally, at the point of the event. If fluorescence is considered, a portion of the approximately 116 keV binding energy of the ejected electron will be emitted as fluorescence X-rays. The portion emitted will be independent of the photons incident energy, i.e., every photoelectric event leads to an ionized atom that will then return to neutrality, independent of how it was ionized.

Even for only a single initial "hole" the relaxation of an atom can involve many radiative and non-radiative transitions. For example, given a single initial vacancy in the K shell of uranium, the vacancy will be filled by an electron transition from another subshell. If the transition is radiative the atom emits a fluorescence X-ray and there will now be one "hole" in the other subshell. If the transition is non-radiative the atom emits an electron and there will now be two "holes" in other subshells. These "holes" will in turn be filled by transitions from other subshells until the atom returns to neutrality. Due to the multiplication of "holes" from non-radiative transitions the result can be a very large number of transitions.

Figs. 5 and 6 illustrate that these spectra can be quite complex. In this case a single "hole" in the K shell of uranium statistically leads to the emission of 154 different energy X-rays and 2772 different energy electrons. Of course in any single given event far fewer X-rays and electrons are emitted, but when averaged over a large number of such events this will be the observed emitted spectra. The most important point to note is that rather than the entire energy being deposited locally, over 89% of the binding energy is re-emitted as fluorescence X-rays. These X-rays are emitted just below photoelectric edges, where the cross sections can be quite small, which allows these X-rays to be quite penetrating. In absolute terms this means that a photoelectric event due to a photon just above the K edge at 116 keV will lead to the emission of about 100 keV of fluorescence X-rays – 89% of its energy; a 1 MeV photon will also result in about 100 keV of fluorescence X-rays – about 10% of its energy, etc. In the case of a 116 keV photon the local deposition will only be 16 keV. However, if fluorescence is not considered, it is assumed to be 116 keV; over 700% higher than the actual value. This over estimation will decrease at higher energies, but even by 1 MeV it will still be about 10% too high. From Fig. 5 we can see that most of the fluorescence X-ray energy will be emitted in a narrow band near 100 keV, just below the K edge where the cross section is only about 25% of the cross section at the top of the K edge, allowing these X-rays to be quite penetrating. For photon transport calculations extending down to energies below several MeV, to realistically model the transport, these fluorescence X-rays should be included in calculations.

This point has been recognized for many years and fluorescence has been included in modern Monte Carlo photon transport codes [7,8]. In these codes the "jump" in the photoelectric cross sections across an edge is used to estimate the fluorescence yield for each subshell.

Now that the photoelectric subshell cross sections are available from EPDL and the fluorescence yield is available from EADL we can use a more detailed model for fluorescence. The subshell cross sections can be used to define what subshell was ionized, and once a subshell is selected our fluorescence yield data can be used to define the emitted X-rays. However, to be able to do this efficiently in calculations we must decide what is or is not important and try to include only those details that are important.

These spectra are judged to be too complicated to sample in detail in applications. However, the most important details can be efficiently sampled. We can use the fact that fluorescence decreases by roughly an order of magnitude for each successive shell. For example, in the case of uranium the fluorescence due to a K shell vacancy is almost 100%, whereas the L shell will be about 10%, the M shell about 1%, etc. In addition we can divide the photon spectrum into those X-rays due to the initial vacancy being filled (what I will refer to as direct or primary X-rays) which are the most energetic X-rays emitted, and those X-rays due to vacancies generated in other shells as the atom relaxes back to neutrality (what I will refer to as secondary X-rays). I will refer to the combination of direct or primary and secondary as the enhanced or total yield.

Fig. 5 illustrates the emitted X-rays (fluorescence) due to a single vacancy in the K shell of uranium. The boxes represent the individual emissions and the solid line represents the integral of the emitted energy spectrum. From this figure we can see that there are 154 individual X-rays emitted, but most of the emissions in terms of probability and energy are in two narrow energy bands just below the K and L edges; these two bands correspond to the direct and secondary fluorescence yields. Based on the integral of the spectrum, in this case the primary fluorescence just below the K edge accounts for about 95% of the emitted X-ray energy and the secondary emission just below the L edge another 4.8%. The entire remainder of the spectrum accounts for only about 0.2% of the emitted X-ray energy, which is small compared to the uncertainty in the emitted spectrum. This suggests that for use in applications rather than attempting to model the entire emitted fluorescence X-ray spectrum all we need model are the two narrow bands of emission just below the K and L edges, in the case of a K shell vacancy; or L and M, for L vacancies; M and N, for M vacancies, etc.

Based on the EADL data, we can calculate [6] the direct and secondary fluorescence yields, both in terms of number of photons and energy emitted as fluorescence for every subshell of every atom ($Z = 1$ through 100). For use in calculations, this data has been reduced to a form where a vacancy in any subshell can result in the emission of up to two fluorescence X-rays where the emission probabilities and energies have been defined to exactly conserve the direct and enhanced fluorescence yields, both in terms of number and energy. These two X-rays per vacancy can accurately model the two narrow bands of emitted X-rays just below the K and L edges that we saw in the Fig. 5.

Since the fluorescence yield decreases rapidly with subshell, an accurate model of fluorescence yield does not require all of the individual subshells to be represented. For use in applications the photoelectric subshell cross sections have been grouped in: K, L1, L2, L3, M, N, O, P, Q, i.e., the most important inner subshells of K and L are represented separately, and the remaining subshells of each shell are grouped together. Furthermore, fluorescence is only considered for K, L1, L2, L3, M and N, which tracks the yield down to a very low level, well below the uncertainty in our atomic relaxation data.

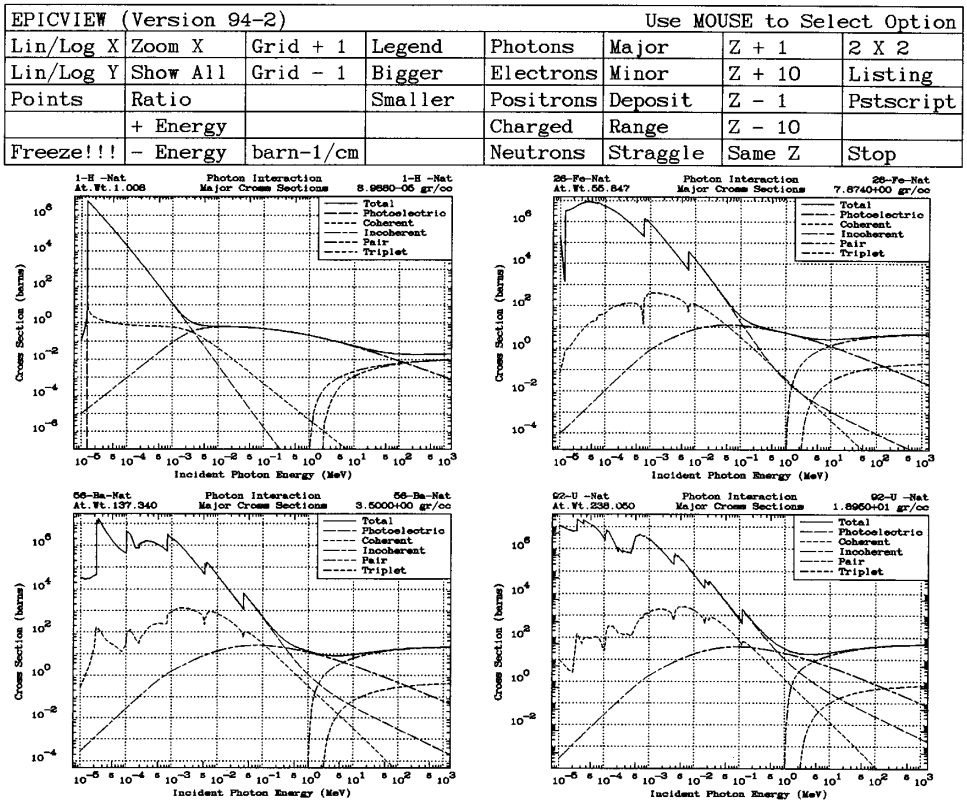

Fig. 7. Example photon cross sections.

Following each photoelectric event we first use the subshell cross sections to randomly select an electron vacancy in a subshell. Once this has been done, the probability of fluorescence yield for that subshell is used to randomly emit X-rays of a given energy; up to two X-rays per primary vacancy are allowed. Even in the extreme case of high Z elements where the K shell fluorescence yield can approach 100%, the two X-rays allowed in this model will track the yield from K shell vacancies down to about 1%. By allowing individual subshells to be sampled the fluorescence will be tracked down even further in energy, e.g., if we had statistically sampled a vacancy in an L subshell the yields could approach about 10% and 1%, tracking the yield down to about 0.1%.

1.6. Pair and triplet production

In the case of pair production, the photon interacts with the field of an entire atom. The photon disappears and an electron–positron pair is created. The sum of the energies of the electron–positron pair is the incident energy of the photon minus the rest mass of the electron–positron pair.

In the case of triplet production the photon interacts with the field of an electron. The photon disappears and an electron–positron pair is created, and an electron is ejected from the atom (leaving an ionized atom). The sum of the energies of the electron–positron pair plus the ejected electron is the incident energy of the photon minus the rest mass of the electron–positron pair and the binding energy of the ejected electron. Compared to the energies of the electron–positron pair, generally the energy of the ejected electron is quite small.

Pair and triplet production are fairly complicated processes, since they are three body processes. For example, in pair production the electron and positron need not equally share the available kinetic energy; indeed at higher energies the spectrum for both becomes quite wide. Here I will merely mention that this spread in the spectra will effect bremsstrahlung emitted by the electron and positron as they slow down in the medium.

Here I will use the simplest possible model for pair and triplet production. I will assume that the electron and positron both slow down and come to rest close to the point of the pair or triplet production event. Therefore, all of their kinetic energy will be deposited locally, and when the positron annihilates two 0.511 MeV photons are created at the point of the pair or triplet event. In the case of triplet production, I will also ignore the low energy ejected electron and the ionized atom.

Later in this paper, I will again discuss pair and triplet under the section What's next?

2. The importance of each process

Fig. 7 illustrates the photon cross sections for four elements spaced across the periodic table. In all cases the variation of the cross sections are smooth functions of Z, so that even from merely these four examples we can see all of the trends of the various cross sections.

Generally, at low energy photoelectric is by far the dominant process. In comparison, the coherent and incoherent cross sections are so much smaller that they are of importance only in special calculations, such as back scattering measurements, where their cross sections may be small, but these are the only processes available to back scatter photons. As described above, at low energy incoherent scattering approaches coherent scattering (no energy loss) and photoelectric is the only effective energy loss process for photons.

At low energies, in high Z elements, fluorescence can be a very important effect, since it can effectively transfer photons from energies above photoelectric edges, where the cross section is high, to energies just below the edges, where the cross section can be much smaller; thereby, allowing these photons to be much more penetrating. Since at low energies the photoelectric cross section can be very large, fluorescence can appear almost to be a surface effect, i.e., most of the photoelectric events above the edges will occur very close to the surface of a high Z element. This will tend to increase the reflection from high Z elements. However, it can also contribute to penetration through materials. For example, in high Z elements the cross section at the bottom of the K edge is about $1/4$ to $1/5$ that of the cross section at the top of the edge. Therefore, if we have a material that based on the cross section at the top of the K edge is say 10 mean free paths thick (we expect little if any transmission), fluorescence can move photons to below the K edge where the material is only 2 to 2.5 mean free paths thick.

At high energies pair and triplet production become the dominant processes. Above about 10 MeV their cross sections are so much larger than the coherent and photoelectric cross sections that the latter can be effectively ignored. Even at fairly high energies incoherent scattering continues to play an important role and should not be ignored. At these high energies coherent and incoherent scattering are very forward peaked, and cause very little back scatter.

At intermediate energies between the high keV and low MeV regions incoherent scattering can be very important. In this energy range the photoelectric cross section has decreased to a small value and the pair and triplet production cross sections have not yet become significant. Therefore, the only effective process that can decrease the energy of photons is incoherent scattering. From Fig. 7 we can see that incoherent scattering in this energy range is particularly important for low Z elements, e.g., hydrogen. At lower energies the incoherent cross section approaches zero as E^2, and becomes dominated by the rapidly increasing photoelectric. Similarly, at higher energies the incoherent cross section decreases, and eventually becomes dominated by the rapidly increasing pair and triplet production cross sections.

Coherent scattering can be an important process in the keV region, in that by scattering photons it will tend to keep them from escaping from a medium, but in no case is coherent scattering the dominant process. At lower energies the coherent cross section approaches zero as E^2, and at higher energies it also decreases toward zero. From Fig. 7 we can see that at low energy coherent is the dominant scattering process. Just below photoelectric edges in high Z elements the coherent cross section can be a significant contribution to the total cross section, e.g., about 10%, that does effect transport.

3. Example results

The purpose of this paper is to introduce the reader to this simple model of photon transport. For acceptance for publication as a journal article this paper has been significantly reduced from its original form which also included a variety of example results. For additional details of this model and example results the reader should see Refs. [9,10] and in particular Ref. [11], which is the original paper.

4. What's next?

The most common assumption used in many photon transport codes is that any energy lost by the photons is deposited locally at the point where each event takes place. In fact, none of the processes that I have discussed in this paper allow photons to directly deposit energy; all that photons can do is transfer their energy to electrons and positrons. In the case of a 20 MeV pair production, do the electron and positron really stop and deposit all of their energy very close to where the pair production occurred, or do they travel and maybe even escape from the medium? The same should be asked of electrons that receive energy from incoherent scattering events. What about feedback? Is it important to consider bremsstrahlung, that will create more photons? What about electron ionization, that can lead to fluorescence?

Because of the coupling between photon and electron, positron transport, without considering the transport of electrons and positrons the picture of photon transport is incomplete. I am not going to even try to cover this topic here. That's what I will cover next: A Simple Model of Electron Transport.

5. Conclusions

In this paper I described a simple model of photon transport. This simple model includes: tabulated cross sections and average expected energy losses for all elements between hydrogen ($Z = 1$) and fermium ($Z = 100$) over the energy range 10 eV to 1 GeV, simple models to analytically describe coherent and incoherent scattering, and a simple model to describe fluorescence. This is all of the data that is required to perform photon transport calculations.

These models have now been implemented in the EPIC (Electron Photon Interaction Code). All of the figures and results presented here are from EPICSHOW [9], an interactive program to allow access to the EPIC data bases, and EPICP [10], a simple photon transport code designed to develop optimum algorithms for later use in EPIC. All of the data described in this paper and all of the programs needed to use it, are available from the author.

Acknowledgements

I thank S.T. Perkins (Lawrence Livermore National Laboratory) and J. Stepanek (Scherrer Institute) for their assistance and many helpful suggestions during the development of this model of photon transport. I also thank Colleen Camacho (Lawrence Livermore National Laboratory) for typing the final form of this paper.

Work performed under the auspices of the US Department of Energy by the Lawrence Livermore National Laboratory under contract nr. W-7405-ENG-48.

References

[1] D.E. Cullen et al., Tables of Graphs of Photon-Interaction Cross Sections from 10 eV to 100 GeV Derived from the LLNL Evaluated Photon Data Library (EPDL), Parts A and B, UCRL-50400, vol. 6, Rev. 4, Oct. 31, 1989, Lawrence Livermore National Laboratory and: S.T. Perkins et al., Tables and Graphs of Atomic Subshell and Relaxation Data Derived from the LLNL Evaluated Atomic Data Library, $Z = 1 - 100$, UCRL-50400, vol. 30, Oct. 31, 1991, Lawrence Livermore National Laboratory

[2] P.F. Rose and C.L. Dunford, ENDF-6 Formats Manual, ENDF-102, Brookhaven National Laboratory.

[3] D.E. Cullen, S.T. Perkins and J.A. Rathkopf, The 1989 Livermore Evaluated Photon Data Library (EPDL), UCRL-ID-103424, March 1990, Lawrence Livermore National Laboratory.

[4] P.P. Kane et al., Phys. Lett. 140 (1986) 85.

[5] J.H. Hubbell et al., Atomic Form Factors, J. Phys. Chem. Ref. Data 4 (3) (1975) 475.

[6] D.E. Cullen, Program RELAX: A Code Designed to Calculate Atomic Relaxation Spectra of s and Electrons, UCRL-ID-110438, March, 1992, Lawrence Livermore National Laboratory.

[7] J.R. Kimlinger, N.L. Monson and E.F. Plechaty, TART and ALICE Input Manual, UCID-17026, Rev. 3, January 1990, Lawrence Livermore National Laboratory.

[8] J.F. Briesmeister, ed., MCNP – A General Monte Carlo Code for Neutron and Photon Transport, Version 3A, LA-

7396-M, Rev. 2, September 1986, Los Alamos National Laboratory.

[9] D.E. Cullen, Program EPICSHOW: A Computer Code to Allow Interactive Viewing of the EPIC Data Libraries, Version 94-1, UCRL-ID-116819, February 1994, Lawrence Livermore National Laboratory.

[10] D.E. Cullen, Program EPICP: Electron Photon Interaction Code: Photon Test Module, UCRL-ID-118400, September 1994, Lawrence Livermore National Laboratory.

[11] D.E. Cullen, A Simple Model of Photon Transport, UCRL-JC-118254, Rev. 1, September 1994, Lawrence Livermore National Laboratory.